Network remodeling induced by transcranial brain stimulation: A computational model of tDCS-triggered cell assembly formation

Abbreviated title: tDCS-triggered cell assembly formation

Han Lu[1,2], Júlia V. Gallinaro[1] and Stefan Rotter[1]

[1] Bernstein Center Freiburg & Faculty of Biology, University of Freiburg, Freiburg, Germany
[2] Institute of Cellular and Integrative Neuroscience, University of Strasbourg, Strasbourg, France

Corresponding author:
Stefan Rotter
Bernstein Center Freiburg
Hansastraße 9a
79104 Freiburg
Germany
stefan.rotter@bio.uni-freiburg.de

Conflict of interests: The authors declare no competing financial interests.
Code Accessibility: Simulation and analysis code is available upon request.

Abstract

Transcranial direct current stimulation (tDCS) is a variant of non-invasive neuromodulation, which promises treatment for diseases like major depressive disorder or chronic pain for patients resistant to conventional therapies. In experiments, long lasting after-effects were observed, suggesting that plastic changes were induced. The exact mechanism underlying the emergence and maintenance of these after-effects, however, remains elusive. Here we propose a model to explain how transcranial stimulation triggers a homeostatic response of the network involving growth and decay of synapses. In our model, the cortical tissue underneath the electrodes is conceived as a recurrent network of excitatory and inhibitory neurons, in which excitatory-to-excitatory synapses are subject to structural plasticity. Various aspects of stimulation were tested via numerical simulations of such networks, including size and montage of the electrode, as well as intensity and duration of the stimulation. Our results suggest that stimulation indeed perturbs the homeostatic equilibrium and leads to cell assembly formation. Strong focal stimulation, for example, enhances the connectivity of new cell assemblies by increasing the rate of synaptic remodeling. Repetitive stimulation with well-chosen duty cycles increases the impact of stimulation as well. The long-term goal of our work is to optimize the impact of tDCS in clinical applications.

Introduction

Transcranial direct current stimulation (tDCS) is a non-invasive brain stimulation technique, where a weak constant current (typically a few mA) is applied to the brain via two or more electrodes attached to the scalp (DaSilva et al., 2011; Edwards et al., 2013). In any tDCS montage, electrical charge is delivered to the brain through an anode and a cathode, which establishes an electric field with a specific geometry (Miranda et al., 2006). Weak electric current passing through the neural tissue and the induced weak electric field are typically not sufficient to trigger action potentials directly, but they are able to either depolarize or hyperpolarize the membrane of single neurons to some degree (Joucla and Yvert, 2009). The membrane potential change, however, can influence spike timing and firing rate of neurons which are part of an active network (Bikson et al., 2006). As a consequence, and similar to other methods of neuromodulation, tDCS is claimed to have a certain potential for treating diseases, such as medication-resistant depressive disorder (Nitsche et al., 2009) or chronic pain (Garcia-Larrea, 2016). It has been shown to have antidepressant effects by targeting the imbalanced activity between the dorsolateral prefrontal cortex of both hemispheres (Loo et al., 2012), and to ameliorate neuropathic pain by targeting primary motor cortex (Ngernyam et al., 2015).

Although there is a record of promising applications of tDCS, it is not yet clear what its underlying neuronal mechanisms are. Immediate changes of neural activity caused by tDCS have been demonstrated both in humans and in rodents. Positron-emission tomography (PET) in humans revealed that tDCS affects the activity in many different brain regions, but the volume directly underneath the stimulation electrodes is influenced most (Lang et al., 2005). Modeling studies have mapped the relation between the amplitude of the applied current, or the induced electric field strength, respectively, and the changes in the membrane potential of neurons (Huang et al., 2017; Datta et al., 2009; Jackson et al., 2016). Experiments in acute hippocampal slices elucidated the relation between the

orientation of the electric field (EF) and the resulting neural activity (Bikson et al., 2004). In contrast to the naive expectation that anodal stimulation increases the activity of the stimulated area, while cathodal stimulation inhibits it, the actual effects appear to depend mainly on the orientation of the EF vector relative to the somato-dendritic axis of neurons (Wiethoff et al., 2014; Gluckman et al., 1996; Radman et al., 2009). When the EF is properly aligned with the somato-dendritic axis (dendrite closer to anode than soma), the somatic membrane potential is depolarized and the neuronal firing rate is increased. For the opposite EF direction, the somatic membrane potential is hyperpolarized and neural activity is attenuated. If the EF is perpendicular to the somato-dendritic orientation, the EF cannot influence the activity of this particular neuron. As a consequence, cells with extended and non-isotropic morphologysuch as pyramidal neurons, should generally be more influenced by tDCS than compact inhibitory neurons. In an effective point neuron model, the polarization induced by an external EF can be equivalently described by a current injected into the soma. This rationale was suggested by the following experimental observation: A uniform EF was able to inhibit KCl-induced epileptiform activity in rat hippocampal slices (Gluckman et al., 1996), but an equivalent effect could be achieved by somatic DC injection (Kayyali and Durand, 1991). An equivalent effect of current injection and EF exposure was also demonstrated in a simulation study (Aspart et al., 2016).

In addition to the instant activity change during stimulation, sustained alterations of neural activity were also observed in humans after turning the stimulation off. The after-effects of tDCS were first reported by Nitsche and Paulus (2000); they used transcranial magnetic stimulation (TMS) triggering motor evoked potentials (MEP) in the right abductor digiti minimi muscle (ADM) as a readout of the after-effects of tDCS in motor cortex. An elevated MEP was reported even 150 min after tDCS application (1 mA) in motor cortex (Nitsche and Paulus, 2001). Such after-effects were later also observed in somatosensory cortex (Matsunaga et al., 2004). Follow-up animal studies suggested that the elevated activity and excitability is not due to reverberating network effects (Gartside, 1968a). Rather, it was observed that synaptic protein synthesis was increased (Gartside, 1968b), which already points to elevated synaptic plasticity. Indeed, blocking brain derived neurotrophic factor (BDNF) (Fritsch et al., 2010), NMDA receptors (Nitsche et al., 2003) or calcium channels (Monte-Silva et al., 2013) reduced the increments of field potential amplitudes in mouse motor cortex induced by tDCS. All of these findings taken together suggest very strongly that the observed after-effects are due to an induction of synaptic plasticity.

Current evidence suggests, however, that multiple forms of plasticity are contributing to tDCS after-effects. Monte-Silva et al. (2013) observed different types of after-effects, linked to different stimulation patterns: Fast facilitation was induced already after a single anodal tDCS session (13 min) and lasted for at least 2 h post stimulation. This phenomenon is called early-LTP (e-LTP). In contrast, 26 min anodal stimulation resulted in a reduced MEP amplitude, pointing towards a homeostatic down-regulation. More interestingly, repetitive anodal tDCS with 20 min pauses interspersed (13 min - 20 min - 13 min) resulted in late facilitation. An elevated MEP was observed only one day after the second stimulation, but not immediately afterwards. This is called late-LTP (l-LTP). These results suggest that both Hebbian and homeostatic, as well as functional and structural forms of plasticity could be involved. Functional LTP-like plastic changes of existing synapses were observed in DCS (Ranieri et al., 2012). Given the time scales of

l-LTP, structural plasticity also seems to play a role in the after-effects. Structural changes at a slower time scale, however, can easily be underestimated due to difficulties measuring spine turnover and changes in dendritic morphology *in vivo*. Homeostatic structural plasticity is constantly taking place in many brain areas (Van Ooyen, 2011; Turrigiano and Nelson, 2004). For example, in adult barrel cortex and visual cortex, whisker trimming or monocular deprivation, respectively, trigger robust spine remodeling (Trachtenberg et al., 2002; Oray et al., 2004). In hippocampal cell cultures, blocking activity with TTX leads to synapse enlargement and synapse cluster formation (Lee et al., 2013). In view of all this, it seems very likely that long-lasting after-effects are caused by structural changes in the network, justifying that we use simulations of spiking neural networks with homeostatic structural plasticity to study them. In this paper, we systematically explore the changes in network activity caused by tDCS, and the network remodeling and cell assembly formation induced by this through a homeostatic response of the network. Our simulations also predict that a focused and/or repetitive stimulation with well-chosen duty cycles can boost the effect. This again fits the experiences from tDCS practice with a high-definition montage (Kuo et al., 2013) and repetitive stimulation (Monte-Silva et al., 2013).

Results

Immediate effect of transcranial stimulation on network activity

As explained in the Introduction, the direct current applied to the brain during tDCS stimulation induces an electric field (EF) (Radman et al., 2009), and may lead to a membrane potential deflection of the soma, depending on the orientation of the EF relative to the neural somato-dendritic axis (Aspart et al., 2016). An equivalent effect with regard to membrane potential modulation is achieved by DC injection into the soma (Kayyali and Durand, 1991). Therefore, in this paper we model tDCS by injecting direct current into the soma of point neurons (Figure 1A) to achieve a small depolarization or hyperpolarization of its membrane potential. The current is compatible with the membrane potential deflection, ΔV, and scaled by a geometric factor reflecting the angle between the EF vector and somato-dendritic axis, θ (Figure 1B). The angle θ determines the injected current according to $\Delta V = \lambda E \cos(\theta)$, where λ is a scaling factor, E is the EF intensity. The equivalent DC to be injected into the neuron is given by Ohm's law $\Delta I = \frac{\Delta V}{R_m}$, where R_m is the membrane resistance. The estimated magnitude of the membrane potential deflection induced by sub-threshold tDCS (1–2 mA) is about 0.1 mV (Jackson et al., 2016), corresponding to 2.5 pA DC injected into the soma of each model neuron.

We then tested if such weak injected current could at all trigger any firing rate changes. We set up a single neuron that generated an ongoing spike train at 8 Hz, as if it was part of a large network. To that end, the ongoing drive from within the network was approximated by a Poisson bombardment. On top of this, we stimulated the neuron by DC injection as described above and observed how the orientation of the EF vector with respect to the orientation of the neuron impacted its firing. Although the overall effect of tDCS stimulation on the membrane potential of the neuron is quite suble, the amplitude of the firing rate change was found to be as large as 1 Hz (Figure 1C).

This very clearly suggests that tDCS can have an appreciable impact on the activity of spiking neurons in a network, even if the stimulation intensity is very weak. As neuronal

spiking is known to affect synaptic connectivity due to activity-dependent plasticity, this raises the question whether direct current stimulation can trigger plastic effects as well. Thus, our next step was to set up a network of point neurons representing the tissue underneath an electrode and find out whether stimulation can alter its structure and its functional dynamics.

Network remodeling triggered by transcranial DC stimulation

We adopt an inhibition-dominated recurrent network of excitatory and inhibitory neurons to represent the cortical tissue underneath the electrodes. The network consists of 10 000 excitatory and 2 500 inhibitory neurons (Brunel, 2000). Neurons are leaky integrate-and-fire (LIF) neurons, with random but fixed 10% E-I, I-I and I-E connection probability (Figure 1D). E-E synapses are grown from scratch, subject to a firing rate based homeostatic structural plasticity rule (Diaz-Pier et al., 2016; Gallinaro and Rotter, 2018). In this model we fix the set-point of the neuronal firing rate at 8 Hz and used a linear homeostatic rule. Eventually, all excitatory neurons fire at 8 Hz, when the connectivity has grown to about 9% (Figure 1F).

In a previous paper, Gallinaro and Rotter (2018) explored the associative properties of a similar network subject to firing rate based homeostatic plasticity. They stimulated a subgroup of excitatory neurons with high-rate external Poisson spike trains. The external stimulation disrupted the homeostatic equilibrium of the subgroup, as increased firing rates above the set point led to a deletion of synapses. When the external stimulation was ceased, the firing rate dropped and homeostatic process robustly triggered synapse formation within the stimulated group. In the work discussed here, tDCS is modeled as weak DC injection into the soma, which causes a change in firing rate of all stimulated neurons. Therefore, we expect similar effects to also happen in the network.

We started by stimulating 10% of all excitatory (1 000) neurons in the network with 2.5 pA DC for 150 s (Figure 2A). When the firing rate of the stimulated group had reached the set-point (same for all neurons), the connectivity also did not change any more with the stimulation. This suggests that the network reached an equilibrium state (see supplementary Figure S1). At this point, we switched the stimulation off and ran the simulation for another 300 s. We also tried different stimulation parameters and compared the effects, as discussed below. As expected, the firing rate of the stimulated group dropped when the DC was turned off (Figure 2B), and this eventually triggered cell assembly formation (Figure 2C). The opposite phenomenon was observed in the process of depolarizing DC (Figure 2D and 2E). Figure 2F illustrates the process of cell assembly formation for the case of 2.5 pA stimulation. Before and after the stimulation, assuming equilibrium in both cases, each neuron receives the same rate of external Poisson input and fires at its target-rate (8 Hz). Thus, the number of input synapses from excitatory neurons should not have changed through stimulation. The only difference will be the source of input synapses: Before the stimulation, input synapses come from both groups of neurons – to be stimulated (blue) and background (empty) – without any bias. The firing rate of the stimulated neurons is most affected, so when stimulation is off, these neurons have more free synaptic elements to offer. Background neurons, which are less affected by stimulation and deviate less from their target rate, can only offer few synaptic elements to form new connections. Since the formation of new synapses is based on the availability of free elements, this leads to a higher probability of connections to be formed within

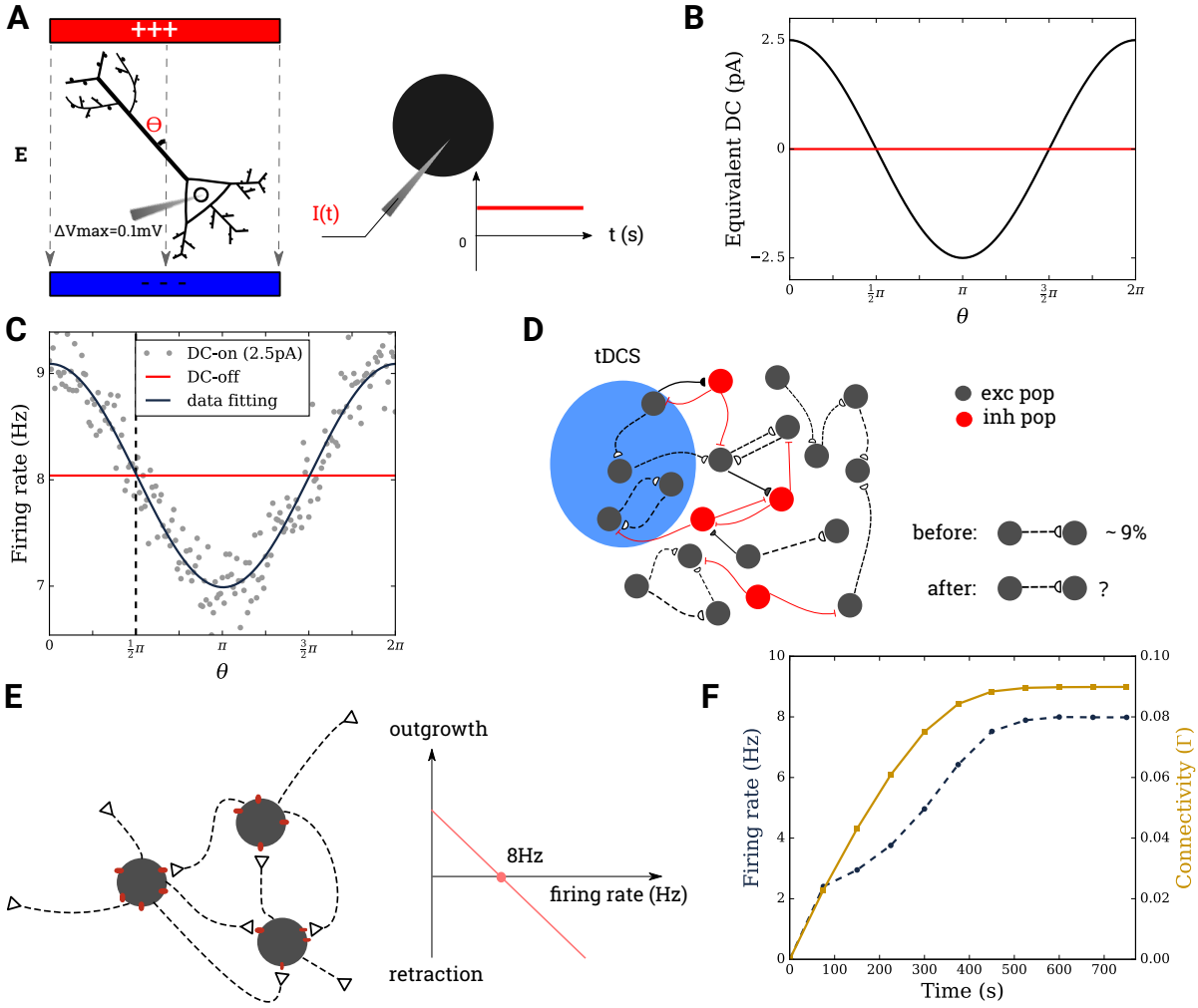

Figure 1: Model of a cortical network underneath the stimulation electrode. **A** The effect of tDCS is realized as direct current injection into the soma of point neurons. **B** The current amplitude depends on the orientation of the electric field vector relative to the somato-dendritic axis. **C** Direct current of amplitude 2.5 pA changes the ongoing firing rate of a single neuron by approx. 1 Hz. **D** The cortical tissue underneath the electrode (blue circle) is modeled as a recurrent network of excitatory and inhibitory neurons. E-I, I-I and I-E connections are static with 10% connectivity, while the E-E connections are subject to homeostatic structural plasticity. **E** The growth and decay of pre-synaptic boutons and post-synaptic spines depends linearly on the neuronal firing rate. Synaptic elements grow or retract as long as the firing rate deviates from the set-point, which was fixed at 8 Hz. **F** The network starts with no E-E connections, whatsoever. After 750 s, the average firing rate has approximately reached the set-point, and the connectivity Γ has settled in a equilibrium at approx. 9%.

the stimulated group. In the case of depolarizing DC the opposite process takes place. Thus, any perturbation to the equilibrium of the network firing rate dynamics, no matter whether it is depolarizing or hyperpolarizing, will trigger synaptic turnover and network remodeling by deleting between-group synapses and forming within-group synapses to form a cell assembly.

The effect of polarity of transcranial DC stimulation

In our model, both depolarizing and hyperpolarizing current stimulation induce cell assembly formation. Due to the different orientations of neurons in real tissue, neurons underneath the same electrode may not be uniformly depolarized or hyperpolarized. Therefore, we examined how a stimulation with mixed polarity performs. In Figure 3 we present two scenarios: bi-population stimulation, in which 30% of the excitatory neurons (G1) are depolarized with 2.5 pA whereas the remaining 70% (G2) are hyperpolarized with -2.5 pA (Figure 3A), and tri-population stimulation, in which 30% of all neurons (G1) are depolarized with 2.5 pA, another group of the same size (G2) are hyperpolarized with -2.5 pA, and the remaining 40% are not stimulated at all. As expected, a combined depolarizing and hyperpolarizing stimulation resulted in higher connectivity within the cell assembly formed (Figure 3C, D and Figure 3E, F).

To further compare the effects of uni-population, bi-population and tri-population stimulation, we performed a systematic study covering different intensities and stimulated group sizes in all three scenarios: bi-group (Figure 4A), uni-group (Figure 4B), and tri-group (Figure 4C). Throughout, we stimulated the network for 150 s and allowed it to relax for 5 850 s to see the persistent change in connectivity. For an unbiased assessment of both short-lived and quasi-permanent effects, We fit the connectivity curve during the relaxation phase with the sum of three exponential functions and calculated the total integral from an extrapolation of the measurement of stimulation effects on connectivity. In the second panel (Figure 4D-F), we show the integral of connectivity over time for the population G1, I_{G_1}, in three scenarios. In each scenario, the integral of connectivity increases with absolute stimulation intensity and decreases with the size of the stimulated population. Strong and focused stimulation leads to strong effects on the connectivity of the cell assembly.

We then performed a comparison between these scenarios A, B and C. When the stimulation is strong and focused, the effect I_{G_1} of scenario B is much stronger than scenario A (Figure 4G) and C (Figure 4H). But when the stimulation is weak, the effect of scenario A is larger than scenario B. Therefore, opposite polarities could slightly boost the cell assembly intensity, if the stimulation is weak. However, for strong and/or focused stimulation, uni-group stimulation leads to stronger cell assemblies. Comparing A and B for strong and focused stimulations, the application of same strength negative DC onto the background in A changes the effect of the same stimulation in B. There might be two aspects involved in this phenomenon. Introducing a DC stimulation of reversed polarity increases the discrepancy between intensies of the stimulated group and the background (from ΔI to $2\Delta I$), but may inhibit the firing due to network inhibitory effects. To disentangle the problem, we fixed the size of the stimulated group G1 as 50% and G2 as 50%, and systematically changed the stimulation intensity for both G1 and G2 in the range between -30 pA and 30 pA. We stimulated G1 and G2 for 150 s and let it relax for 5 850 s. The effects were estimated again as the integral of connectivity over time during

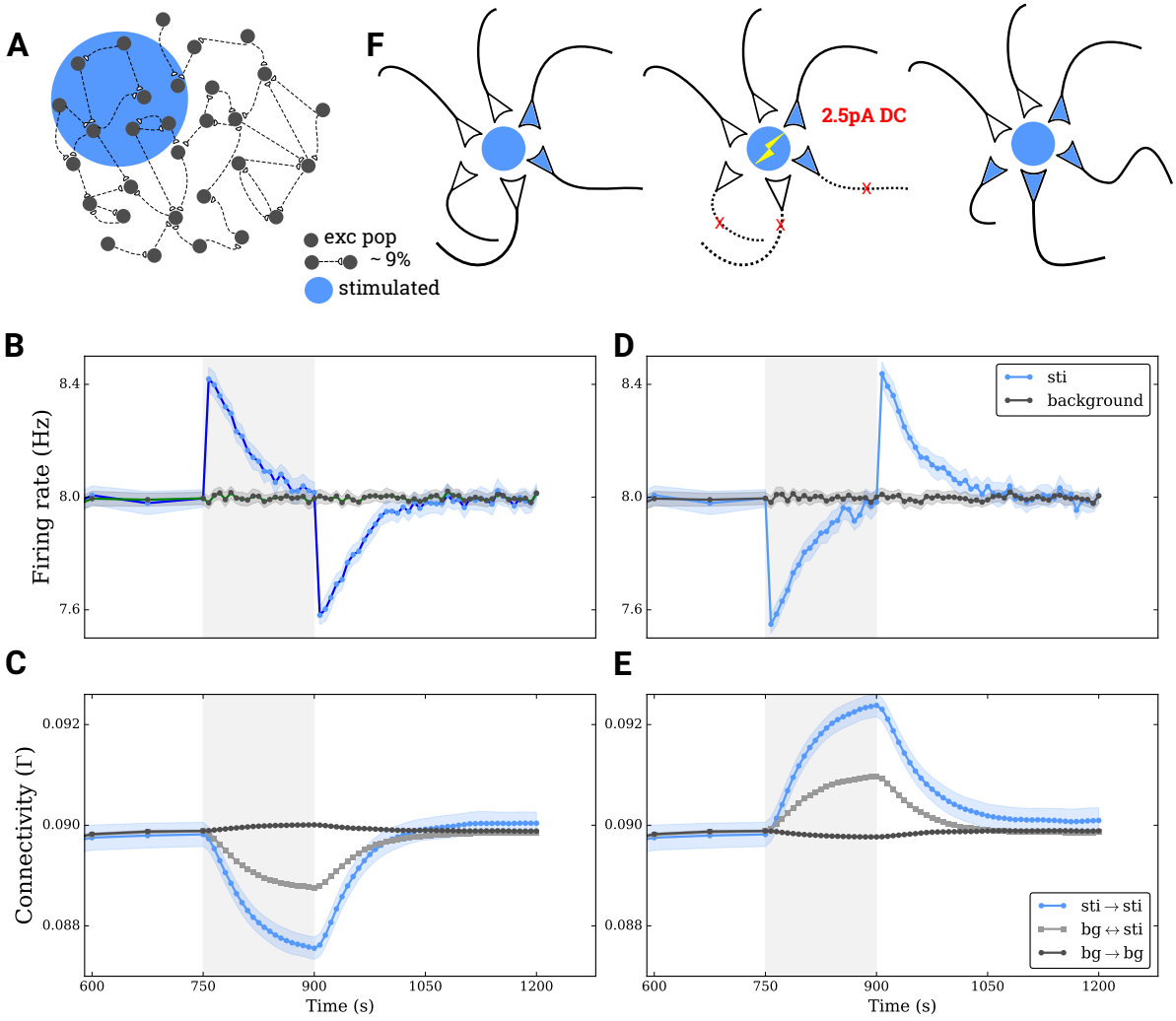

Figure 2: Effects of anodal (depolarizing) and cathodal (hyperpolarizing) tDCS in a recurrent network. **A** A subgroup comprising 10% of all excitatory neurons in a larger network is stimulated by tDCS. Excitatory neurons are more susceptible to stimulation due to their extended non-isotropic morphology, and in our model tDCS has no effect on inhibitory neurons. **B** Average firing rate of directly stimulated (blue) and non-stimulated (grey) excitatory neurons before, during and after stimulation. **C** Average connectivity among stimulated neurons (blue), among non-stimulated neurons (dark grey), and between neurons in different groups (light grey). When depolarizing current is applied, the resulting increase of the firing rate leads to a homeostatic response of the network in terms of a drop in connectivity. When the current is off, the resulting decrease of the firing rates triggers synaptic growth and cell assembly formation. **D**, **E** Similar to **B**, **C**, but for hyperpolarizing current injection. Note that both depolarization and hyperpolarization induced a small but persistent increase of the connectivity, corresponding to the formation of a cell assembly. **F** Before and after the stimulation, when an equilibrium is maintained with the same external input, the excitatory indegree of each neuron will be the same. A transient perturbation of the equilibrium by stimulation facilitates, with some delay, the deletion of synapses originating from non-stimulated neurons and the formation of new synapses from stimulated neurons. This leads to the formation of cell assemblies. Shaded areas on **B**, **C**, **D** and **E** indicate the stimulation period.

the relaxation phase. The final integral of G1 connectivity is plotted in Figure 4I. The values along the diagonal are very small, because there was neither synapse reorganization nor cell assembly formation in these conditions. The remaining integrals are symmetric along the diagonal. When the discrepancy between the two populations is large, close to the two corners for example, the integral of G1 connectivity is also large. We fixed the discrepancy between the pair of stimulation intensities and compare pairs: −30pA and −10pA, −20pA and 0pA, −10pA and 10pA. As shown in the white square in Figure 4I, when the discrepancy is fixed to −20pA, the integral of −20pA and 0pA situation is larger than both −30pA and −10pA, and −10pA and 10pA case. The same tendency was observed in 20pA discrepancy case. This supports the idea that network effects might influence the interaction between two groups, and that uni-group stimulation scenario achieves larger effects when stimulation is strong and focused.

The effect of repeated transcranial DC stimulation

To examine the effects of repetitive stimulation, we repeated the 2.5 pA DC stimulation in a 10% subpopulation with different stimulation time (t_1) and relaxation interval (t_2) (Figure 5A). An example with $t_1 = 150$ s and $t_2 = 150$ s is shown in Figure 5B and 5C. Connectivity generally increases with repetition. Figure 5D summarizes different t_1 and t_2 combinations. Compared to the basic condition, $t_1 = 150$ s, $t_2 = 150$ s, an increase in relaxation time (t_2) of 300 s led to higher connectivity than an increase in the stimulation time (t_1) to 300 s. Therefore, we conclude that repetitive stimulation typically increases the effect of tDCS on cell assembly connectivity. But will it keep rising or saturate eventually? To answer this question, we should simulate the repetitive 2.5 pA tDCS for a long-enough time and check if connectivity eventually saturates. This, however, requires very long simulation times. In order to avoid these long simulations, we used the most effective combination ($t_1 = 150$ s and $t_2 = 300$ s) and replaced the repetitive intensity with a stronger yet still sub-threshold DC intensity (30 pA) to achieve larger connectivity increment in each cycle and approximate the saturation level faster. After several repetitions of 30 pA stimulation, the connectivity seems to saturate at a relatively high level (Figure 5E). Different t_1 and t_2 combinations have slightly different saturation levels.

Since simple on-off repetitive stimulation could boost cell assembly formation, we wondered if replacing the relaxation phase with an opposite current stimulation would further accelerate the process. We adopted two alternating stimulation patterns (Figure 6A) by applying step currents with alternating polarities (±2.5 pA or ±1.25 pA) to 10% excitatory neurons with the same stimulation interval ($t = 150$ s). As Figure 6B and 6C shows, after three repetitions, alternative stimulation with ±2.5 pA accelerated the connectivity when compared to on-off stimulation. However, ±1.25 pA alternating stimulation results in same effects as the on-off stimulation. The cell assembly connectivity after 3 repetition cycles depends on the amplitude of the stimulation pulse, but not on whether it is an on-off or alternative protocol. Figure 6D summarizes the histogram (or the mean and standard deviation, plotted in the inset) of the final connectivity of 30 independent trails at the end of three repetitions, the ±2.5 pA alternative repetition pattern achieves higher connectivity.

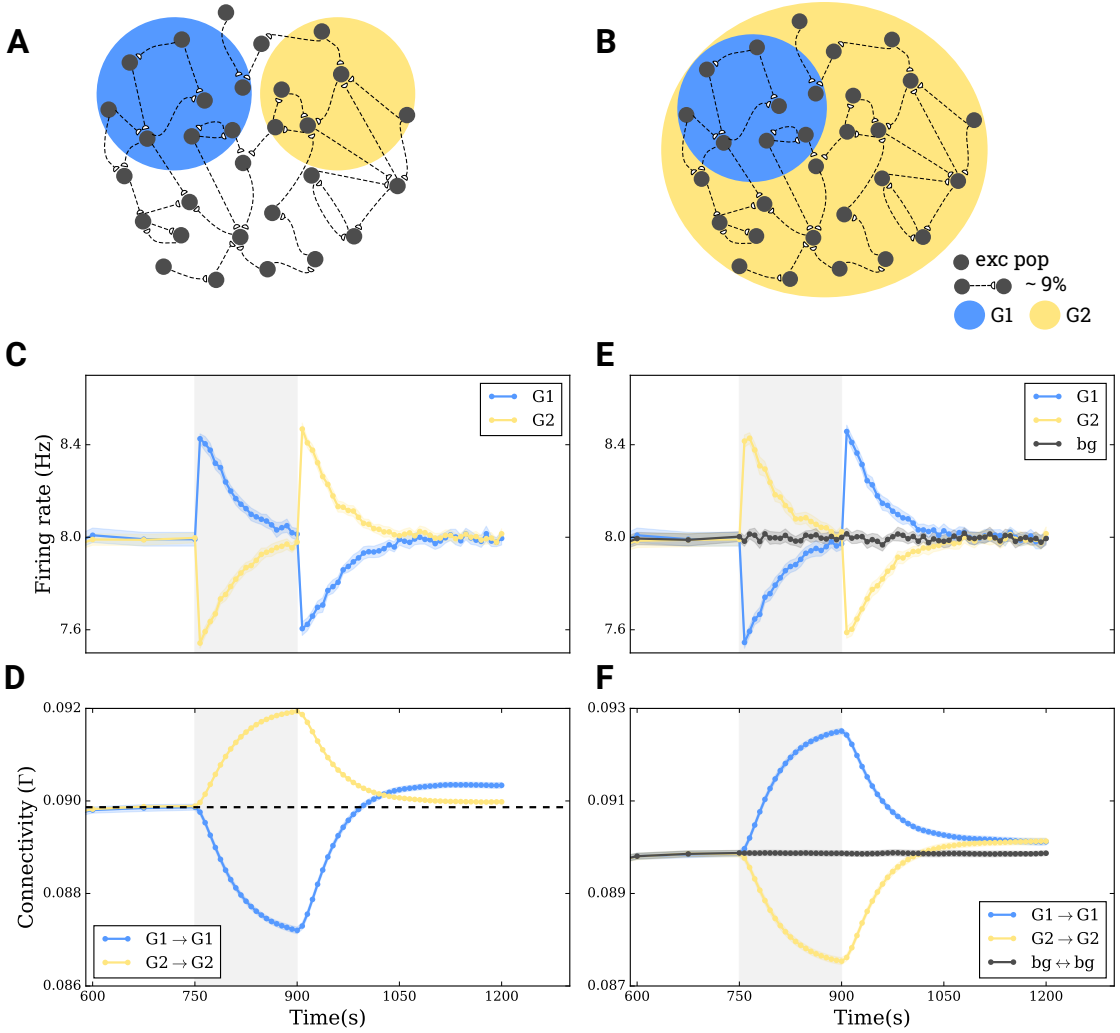

Figure 3: Simultaneous depolarizing and hyperpolarizing tDCS in a recurrent network. To understand the interaction between DC stimuli of different polarity, we apply depolarizing and hyperpolarizing currents to two different subgroups, respectively. Two scenarios are tested: **A** 30% of all neurons in a network (G1) are depolarized with 2.5 pA, another 30% (G2) are hyperpolarized with −2.5 pA, and the rest of 40% receives no stimulus. **B** 30% (G1) are hyperpolarized with 2.5 pA, and the remaining 70% (G2) are depolarized with −2.5 pA. **C**, **E** Group averages of firing rates in G1 (blue) and in G2 (yellow) before, during and after stimulation. **D**, **F** Group averages of the connectivity within G1 (blue), within G2 (yellow) and between G1 and G2 (grey). In both scenarios, cell assemblies were formed both within G1 and within G2.

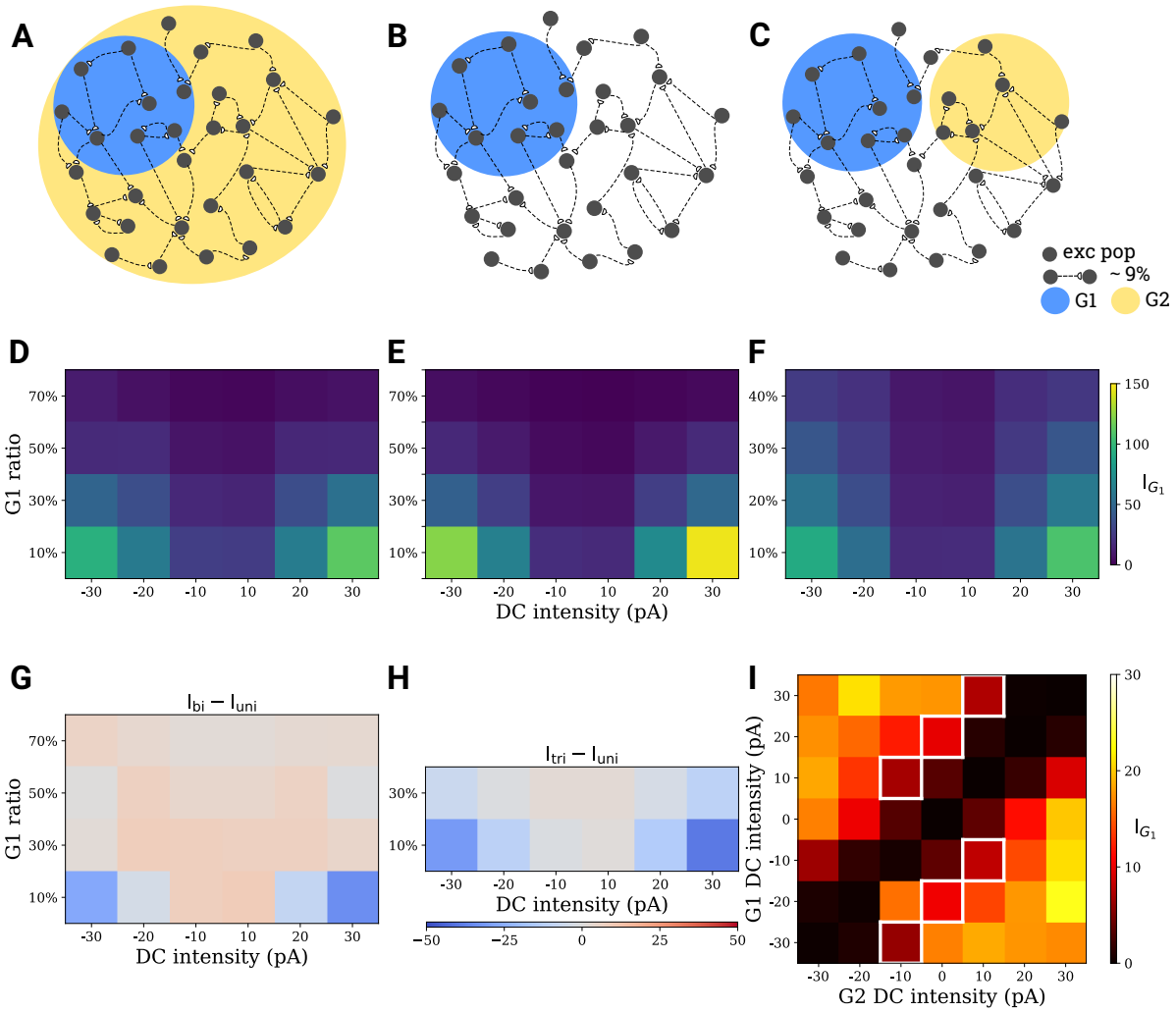

Figure 4: Comparison of tDCS effects in three different stimulation scenarios. **A** Bi-group stimulation: A subpopulation (G1) is stimulated with one polarity and all other excitatory neurons (G2) are stimulated with the opposite polarity. **B** Uni-group stimulation: A subpopulation (G1) is stimulated, and all remaining excitatory neurons receive no stimulus. **C** Tri-group stimulation: G1 and G2 have the same population size and are stimulated by opposite DC, while all other excitatory neurons receive no stimulus. **D** Effect of tDCS on cell assembly formation for scenario **A**, assuming different current amplitude and different relative sizes of the G1 population.The effects on cell assembly connectivity were measured as the integral (I_{G_1}) of the fitted connectivity curve above baseline after turning the stimulus off (see text for details). **E**, **F** Similar to **D** for scenarios **B** and **C** respectively. In all simulations, the network was stimulated for 150 s and relaxed for 5 850 s. Note that the stimulus polarity has almost no effect on the induced connectivity change. **G**, **H** Difference between **D** and **E**, as well as **F** and **E**, respectively. We found that the increased contrast provided by the opposite polarity generally boosted cell assembly connectivity. **I** We now made G1 and G2 equal in size and only changed the DC amplitude. We stimulated the network for 150 s and allowed it to relax for 5 850 s. The effects were measured in the same way as for **D**-**F**. We found that the larger the discrepancy of stimulus strength is between two populations, the stronger the effect on the emerging connectivity is. The white squares indicate the same stimulus discrepancy between neuronal groups. The combination −20 pA and 0 pA yielded stronger effects than −30 pA and −10 pA, or −10 pA and +10 pA.

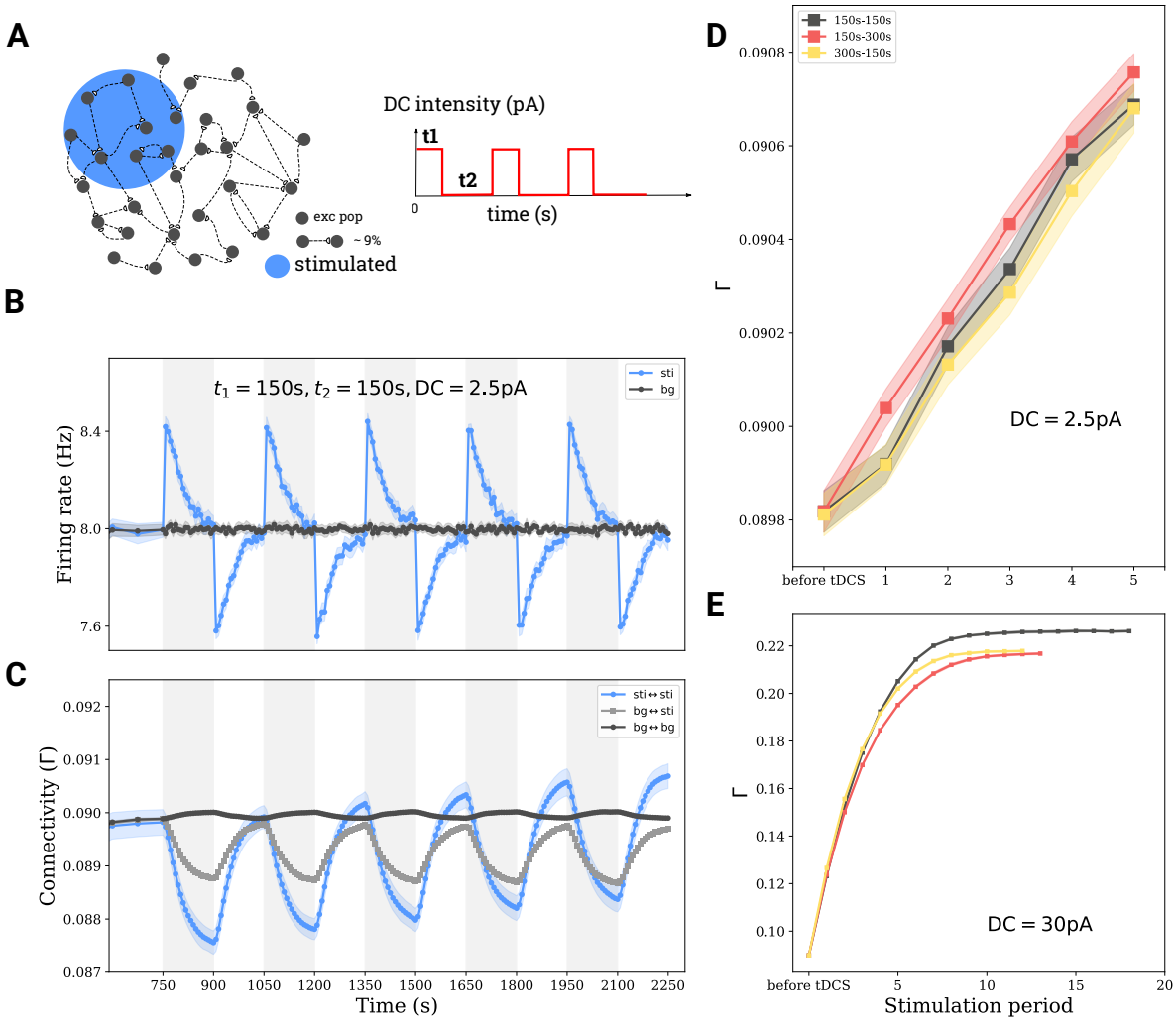

Figure 5: Repetitive stimulation boosts network remodeling. **A** The network is stimulated with a train of DC stimuli. Stimulation time is t_1, followed by a pause of duration t_2. **B** and **C** Average firing rate and connectivity during a train of stimuli. Repetitive stimulation of a subnetwork (10% of all excitatory neurons) with interspersed pauses boosts the connectivity of the cell assembly. **D** The effects depend on the stimulation time (t_1) and the relaxation interval (t_2). We tried different combinations of stimulation and relaxation times. The most efficient stimulation protocol is the shortest duty cycle that still allows the network to reach its structural equilibrium during and after the stimulation. **E** The connectivity increases linearly for the first few cycles and finally saturates at relatively high connectivity values. The DC amplitude was 30 pA for **E**, and 2.5 pA for all other subplots.

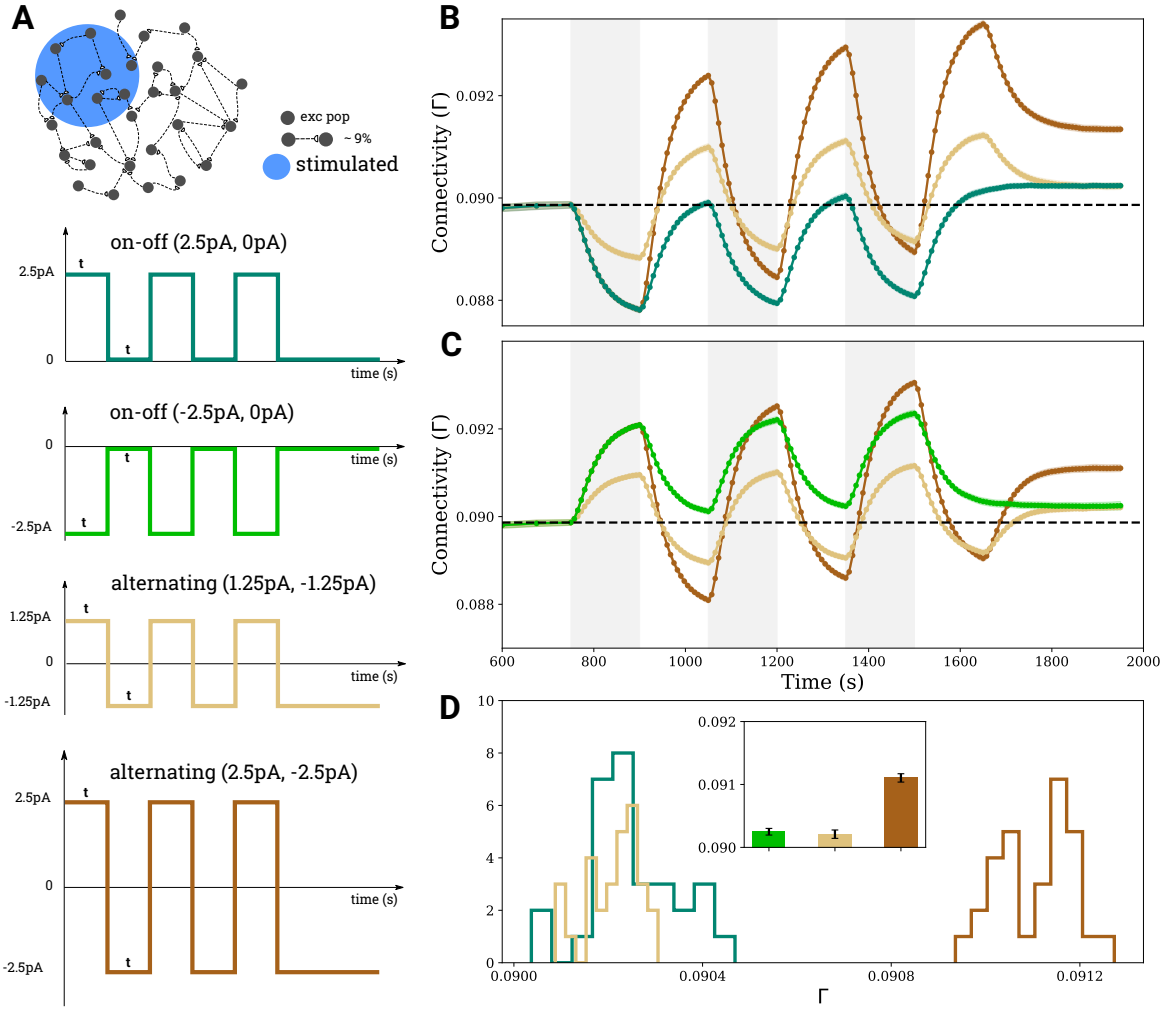

Figure 6: Comparison of four different scenarios for repetitive DC stimulation. **A** 10% of all neurons in the excitatory population were stimulated, using the same duty cycles in each case. However, different amplitudes and polarities were considered, as indicated by the four different curves. **B** and **C** Evolution of average connectivity for the different stimulation scenarios, colors match the stimulus curves in panel **A**. Alternating stimulation with ± 2.5 pA amplitudes (brown) lead to higher connectivity than the 2.5 pA on-off stimulation (light and dark green), while ± 1.25 pA alternating stimulation (orange) yielded roughly the same effects as an on-off stimulation with the same total amplitude (light and dark green). **D** Histograms of the connectivity reached after 3 cycles in the different scenarios extracted from 30 independent simulations. The inset shows mean and variance corresponding to the histograms.

Discussion

In the present study, we explored the plastic changes in network structure that could be induced by transcranial direct current stimulation (tDCS). We demonstrated that even relatively weak sub-threshold direct current stimulation can modulate the firing rate of a neuron that is part of an active network. This modulation can trigger network remodeling and cell assembly formation, if the network is subject to homeostatic structural plasticity. There is, in fact, strong evidence that activity-dependent network remodeling takes place in brains of all ages. We explored different parameters of tDCS stimulation with the help of our model and found that focused strong stimulation could enhance the newly formed cell assemblies. We also found that repetitive stimulation with well-chosen duty cycles could boost the induced structural changes, and repetitive stimulation with alternating sign may achieve even higher connectivity.

In our current study, we used connectivity as a direct readout of stimulation effects. Although there are currently no empirical data that directly demonstrate that structural changes arise as a consequence of stimulation, the factors that we found amplify its effects are not unheard of in tDCS practice. Strong focused stimulation, for example, which corresponds to a high-definition electrode montage, does indeed lead to a stronger MEP and potentiates the therapeutic effects as compared to the conventional montage (Kuo et al., 2013). Applying the same total current, the high-definition montage induces stronger electric fields in smaller brain volumes as compared to the conventional montage (Edwards et al., 2013). As predicted by our model, a stronger electric field will polarize the membrane potential more, induce stronger firing rate responses and, therefore, lead to higher connectivity in the stimulated region. Moreover, a high-definition montage narrows down the affected brain region, and in our model this also contributes to higher connectivity. Repetitive stimulation, another factor predicted to boost connectivity, is already widely used in tDCS practice. As already mentioned in the Introduction, Monte-Silva et al. (2013) demonstrated that an interrupted 13 min - 20 min - 13 min stimulation yielded higher MEP after-effects than a single uninterrupted 26 min stimulation, while a repetition with a very long pause between stimulation episodes (13 min - 24 h - 13 min) did not accumulate the after-effects at all. The inter-stimulation interval and duty cycle does matter. In our model, the effective interval should be long enough for the system to recover its equilibrium firing rate and homeostatically respond by changing the connectivity, but not too long for the connectivity to decay to the unperturbed level again. In our simulations, we found a $1:2$ ratio for the ON-OFF period length to be highly efficient, very similar to what Monte-Silva et al. (2013) reported.

Other computational approaches have previously been suggested to analyze the tDCS mechanism. In experiments performed both in brain slices and human subjects, the mechanistic understanding approached the level how tDCS/DCS could influence the electric activity of the brain at the single neuron level. Most notably, Bikson et al. (2006) has explored several very different aspects that may also contribute to tDCS function: potassium concentration, inhibitory neurons, action potential timing, and polarization of the axonal terminal. Most experimental and theoretical studies nowadays emphasize the role of excitatory neurons. Joucla and Yvert (2009) came up with the mirror estimation of membrane potential changes for large axons in the electric field, and Aspart et al. (2016) conceived the influence of the electric field on neuronal dendrites as external input to the soma. Another computational approach based on modern structural brain imaging

methods maps the current distribution onto the whole brain and provides answers to the question how strong the stimulation effects actually are. Spherical head models were first used to estimate the 3D current flow for any given electrode montage (Miranda et al., 2006). Then fMRI based individualized modeling was employed for treating stroke and depressive patients (Datta et al., 2009; Ho et al., 2014; Huang et al., 2017). Our current work also adopted the parameters from both experiments and estimations made by such approaches. We provide a new and original computational model to explore the plasticity at the network level, which bridges two approaches, from the level of single neurons to networks.

We should interpret the results and predictions of our work on network remodeling induced by tDCS with due caution. Although we know that homeostatic structural plasticity is extremely robust for a wide range of time scales (Gallinaro and Rotter, 2018), an exact match of the plasticity dynamics has not been attempted here. Also, considering only one type of plasticity is very likely a great simplification as compared to real brain networks. As shown by Monte-Silva et al. (2013) in experiments, different repetitive stimulation patterns triggered either early-LTP or late-LTP like phenomena; the non-linearity of intensity dependent after-effects reported by Jamil et al. (2017) also suggested a more complicated interaction. Our structural plasticity rule may fit the time scale of late-LTP, but not of early-LTP. The latter often sets in right after the anodal tDCS was turned off and lasts for at least two hours post stimulation, suggesting that Hebbian plasticity on a fast time scale is also involved. Therefore, a closer look at the interplay between fast functional plasticity and slow structural plasticity will be necessary to fully understand the inner logic of stimulation after-effects. On the other hand, there are still important factors that are not at all addressed by our computational approach yet. Astrocytes, for instance, were reported to be involved in the Ca^{2+} signaling and synaptic plasticity during tDCS (Monai and Hirase, 2017), but this is not yet reflected in our model. Moreover, the link between cell assembly connectivity, enhanced function and changed behavior (e.g. improved cognition and/or ameliorated depressive symptoms) is far from clear. Our current work, however, could be a first step toward the goal of devising optimized tDCS protocols.

Methods

Neuron model

All large-scale simulations of plastic neuronal networks of this study were performed with the NEST simulator (Bos et al., 2015). The current-based leaky integrate-and-fire neuron model was used throughout. This model is described by

$$\tau_m \frac{\mathrm{d}V_i}{\mathrm{dt}} = -V_i + \tau_m \sum_j J_{ij} S_j(t-d) + I_i^{\mathrm{ext}} \tag{1}$$

where τ_m is the membrane time constant. The variable $V_i(t)$ is the membrane potential of neuron i, the resting value of which is set to 0 mV. I_i^{ext} comprises external inputs. The spike train generated by neuron i is denoted by $S_i(t) = \sum_k \delta(t - t_i^k)$, where t_i^k represent the individual spike times. The entries of the matrix J_{ij} denote the amplitude of the postsynaptic potential that is induced in neuron i upon the arrival of a spike from neuron

j. In our model, excitatory synapses have the amplitude $J_E = 0.1\,\mathrm{mV}$, whereas inhibitory synapses have an amplitude of $J_I = -0.8\,\mathrm{mV}$. When the membrane potential reaches the firing threshold, V_{th}, an action potential is generated and the membrane potential is reset to $V_{\mathrm{reset}} = 10\,\mathrm{mV}$. All parameters are again listed in Table 1.

Network model

The network underneath the stimulation electrode is conceived as an inhibition-dominated recurrent network (Brunel, 2000), comprising 10 000 excitatory and 2 500 inhibitory neurons. All E-I, I-E, I-I connections are static and synapses have a fixed synaptic weight J_E or J_I, respectively. All these connections are randomly established, with 10% connection probability. In contrast, E-E connections are subject to a growth rule called homeostatic structural plasticity (Gallinaro and Rotter, 2018; Butz and van Ooyen, 2013; Diaz-Pier et al., 2016). The network has initially no E-E connections, they are grown according to the specified rule. Each neuron in the network receives Poisson external input at a rate of $r_{\mathrm{ext}} = 30\,\mathrm{kHz}$. For the parameters chosen here, the network enters an asynchronous-irregular state (Brunel, 2000). All network parameters are again listed in Table 2.

Homeostatic structural plasticity

As pointed out before, E-I, I-E, I-I connections have static synapses with $J_E = 0.1\,\mathrm{mV}$ for excitatory synapses and $J_I = -0.8\mathrm{mV}$ for inhibitory synapses. E-E connections undergo continuous remodeling, governed by a firing rate based homeostatic structural plasticity rule. Excitatory synapses are formed by combining a pre-synaptic bouton and a post-synaptic spine, the so-called synaptic elements. New synapses can form only if free synaptic elements are available. Pairs of neurons can form multiple synapses between them, where each individual synapse has the same weight of $J_E = 0.1\,\mathrm{mV}$. It has been observed in experiments that neurite growth is governed by the concentration of intracellular calcium. A specific hypothesis states that there is a set-point of the calcium concentration, which the neuron strives to reach (Ramakers et al., 2001; Mattson and Kater, 1987). In the model of structural plasticity we use in our work, the growth and deletion of synaptic elements is linked to the time-dependent intracellular calcium concentration $C(t) = [\mathrm{Ca}^{2+}]$ of the neuron in question. In fact, this variable is a good indicator of the neuron's firing rate (Grewe et al., 2010): Whenever the neuron generates a spike as represented by the spike train $S(t)$, the intracellular calcium concentration experiences an increase by the amount β_{Ca} through calcium influx. In between two steps, the calcium concentration decays exponentially with time constant τ_{Ca}

$$\frac{\mathrm{d}C(t)}{\mathrm{d}t} = -\frac{1}{\tau_{\mathrm{Ca}}}C(t) + \beta_{\mathrm{Ca}}S(t). \tag{2}$$

The synaptic growth rule is now as follows: When the firing rate (or calcium concentration) is below its set-point, the neuron will grow new synaptic elements to compensate for the lack of input. Existing synapses are broken up and synaptic elements are added to the pool of free synaptic elements, if the firing rate is above the set-point. We adopted a liner growth rule for both presynaptic and postsynaptic elements (Gallinaro and Rotter,

2018)

$$\frac{\mathrm{d}z}{\mathrm{d}t} = \nu\big[1 - \frac{1}{\epsilon}C(t)\big], \tag{3}$$

where z is the number of (presynaptic or postsynaptic) elements, ν is the growth rate, and ϵ is the target level of calcium concentration, measured in arbitrary units. In any given moment, free synaptic elements are randomly combined into new functional synapses. All the parameters defining the structural plasticity rule are listed in Table 3.

Measurements and calculations

Firing rate.

The firing rate of a neuron is calculated as its time-averaged spike count, based on 5 s activity recording. The mean firing rate in a population is the arithmetic mean of firing rates across neurons in the group.

Synaptic connectivity.

The connectivity, Γ, is calculated as the mean number of synapses per pair of neurons in a certain group. Let (A_{ij}) be the $n \times n$ connectivity matrix of a network with n neurons. Its columns correspond to the axons, its rows correspond to the dendrites of the neurons involved. The specific entry A_{ij} of this matrix represents the total number of synapses from the presynaptic neuron j to the postsynaptic neuron i. The mean connectivity of this network is then given by $\Gamma = \frac{1}{n^2}\sum_{ij} A_{ij}$.

Time integral of the connectivity.

When comparing the effects of different stimulation scenarios, one cannot simply compare the connectivity of the cell assembly at the end of simulation, because the connectivity decays with different time constants. Therefore, we fit the connectivity change over time during the relaxation phase by a sum of three exponential decay functions

$$\Gamma(t) = A_1 \exp^{-t/\tau 1} + A_2 exp^{-t/\tau_2} + A_3 \exp^{-t/\tau_3}. \tag{4}$$

The parameter A_k is the amplitude of a component that decays with time constant τ_k. We calculated the total integral of the connectivity by extrapolation $I_G = \sum_k A_k \tau_k$. This way we can also account for connectivity transients that persist for a very long time, beyond the duration of our simulations.

Stimulation parameters.

In our study we tested different DC stimulation scenarios. All stimulation parameters are summarized in Table 4.

Table 1: Parameters of neuron model

τ_m	t_{ref}	V_0	V_{reset}	V_{th}
10.0 ms	2.0 ms	0.0 mV	10.0 mV	20.0 mV

Table 2: Parameters of network model

N_E	N_I	Γ_{E-I}	Γ_{I-E}	Γ_{I-I}	J_E	J_I	r_{ext}
10 000	2 500	10%	10%	10%	0.1 mV	−0.8 mV	30 kHz

Table 3: Parameters of the structural plasticity model

ϵ	ν	τ_{Ca}	β_{Ca}
0.008	$0.004\,\text{s}^{-1}$	10 s	0.0001

Supportive Information

Authorcontributions

The project was planned and realized by HL, JG, SR. JG established the network model with homeostatic structural plasticity. HL formalized the model of tDCS and performed all numerical simulations. HL analyzed the data; JR and SR contributed to the data analysis. HL wrote the manuscript, and all authors contributed to the revision.

Acknowledgments

This work is funded by the Universitätsklinikum Freiburg and NEUREX. Additional support by the German Research Foundation (DFG) through EXC 1086, and by the state of Baden-Württemberg through bwHPC and the German Research Foundation (DFG) through INST 39/963-1 FUGG is acknowledged. The authors thank Claus Normann, Lukas Frase, Andre Russowsky Brunoni, and Benjamin Merkt for useful discussions. We also thank Uwe Grauer from the Bernstein Center Freiburg as well as Bernd Wiebelt and Michael Janczyk from the Freiburg University Computing Center for their assistance with HPC applications.

Table 4: Configurations of DC stimulation

protocol	f_{G1}	I_{G1} [pA]	f_{G2}	I_{G2} [pA]	f_{G3}	I_{G3} [pA]	growth [s]	repetition	stimulation [s]	relaxation [s]
Figure 2B	10%	2.5	90%	0	-	-	750	no	150	300
Figure 2D	10%	2.5	90%	0	-	-	750	no	150	300
Figure 3A	30%	2.5	30%	-2.5	40%	0	750	no	150	300
Figure 3B	30%	2.5	70%	-2.5	-	-	750	no	150	300
Figure 4A	10%, 70% [1]	-30, 30 [2]	$1-f_{G1}$	$-I_{G1}$	-	-	750	no	150	5 850
Figure 4B	10%, 70%	-30, 30	$1-f_{G1}$	0	-	-	750	no	150	5 850
Figure 4C	10%, 40% [3]	-30, 30	f_{G1}	$-I_{G1}$	$1-f_{G1}-f_{G2}$	0	750	no	150	5 850
Figure 4I	50%	-30, 30	50%	$-I_{G1}$	-	-	750	no	150	5 850
Figure 5	10%	2.5, 30	90%	0	-	-	750	yes	multiple[4]	
Figure 6-on-off	10%	2.5	90%	0	-	-	750	yes	150	150
Figure 6-on-off	10%	-2.5	90%	0	-	-	750	yes	150	150
Figure 6-alternating	10%	± 1.25	90%	0	-	-	750	yes	150	150
Figure 6-alternating	10%	± 2.5	90%	0	-	-	750	yes	150	150

[1] The stimulation ratios are 10%, 30%, 50%, 70%

[2] The stimulation intensities are -30, -20, -10, 10, 20, 30 pA

[3] The stimulation ratios are 10%, 20%, 30%, 40%

[4] The combinations used are $(150, 150)$, $(150, 300)$, $(300, 150)$ s.

All results in this study except Figure 4I are averages from 30 independent simulations.

References

Aspart, F., Ladenbauer, J., and Obermayer, K. (2016). Extending integrate-and-fire model neurons to account for the effects of weak electric fields and input filtering mediated by the dendrite. *PLoS computational biology*, 12(11):e1005206.

Bikson, M., Inoue, M., Akiyama, H., Deans, J. K., Fox, J. E., Miyakawa, H., and Jefferys, J. G. (2004). Effects of uniform extracellular dc electric fields on excitability in rat hippocampal slices in vitro. *The Journal of physiology*, 557(1):175–190.

Bikson, M., Radman, T., and Datta, A. (2006). Rational modulation of neuronal processing with applied electric fields. In *Engineering in Medicine and Biology Society, 2006. EMBS'06. 28th Annual International Conference of the IEEE*, pages 1616–1619. IEEE.

Bos, H., Morrison, A., Peyser, A., Hahne, J., Helias, M., Kunkel, S., Ippen, T., Eppler, J. M., Schmidt, M., Seeholzer, A., and et al. (2015). Nest 2.10.0.

Brunel, N. (2000). Dynamics of sparsely connected networks of excitatory and inhibitory spiking neurons. *Journal of computational neuroscience*, 8(3):183–208.

Butz, M. and van Ooyen, A. (2013). A simple rule for dendritic spine and axonal bouton formation can account for cortical reorganization after focal retinal lesions. *PLoS computational biology*, 9(10):e1003259.

DaSilva, A. F., Volz, M. S., Bikson, M., and Fregni, F. (2011). Electrode positioning and montage in transcranial direct current stimulation. *J Vis Exp*, (51).

Datta, A., Bansal, V., Diaz, J., Patel, J., Reato, D., and Bikson, M. (2009). Gyri-precise head model of transcranial direct current stimulation: improved spatial focality using a ring electrode versus conventional rectangular pad. *Brain Stimulation: Basic, Translational, and Clinical Research in Neuromodulation*, 2(4):201–207.

Diaz-Pier, S., Naveau, M., Ostendorf, M., and Morrison, A. (2016). Automatic generation of connectivity for large-scale neuronal network models through structural plasticity. *Frontiers in neuroanatomy*, 10:57.

Edwards, D., Cortes, M., Datta, A., Minhas, P., Wassermann, E. M., and Bikson, M. (2013). Physiological and modeling evidence for focal transcranial electrical brain stimulation in humans: a basis for high-definition tdcs. *Neuroimage*, 74:266–275.

Fritsch, B., Reis, J., Martinowich, K., Schambra, H. M., Ji, Y., Cohen, L. G., and Lu, B. (2010). Direct current stimulation promotes bdnf-dependent synaptic plasticity: potential implications for motor learning. *Neuron*, 66(2):198–204.

Gallinaro, J. V. and Rotter, S. (2018). Associative properties of structural plasticity based on firing rate homeostasis in recurrent neuronal networks. *Scientific reports*, 8(1):3754.

Garcia-Larrea, L. (2016). tdcs as a procedure for chronic pain relief. *Neurophysiologie Clinique/Clinical Neurophysiology*, 46(3):224.

Gartside, I. B. (1968a). Mechanisms of sustained increases of firing rate of neurones in the rat cerebral cortex after polarization: reverberating circuits or modification of synaptic conductance? *Nature*, 220(5165):382.

Gartside, I. B. (1968b). Mechanisms of sustained increases of firing rate of neurones in the rat cerebral cortex after polarization: role of protein synthesis. *Nature*, 220(5165):383.

Gluckman, B. J., Neel, E. J., Netoff, T. I., Ditto, W. L., Spano, M. L., and Schiff, S. J. (1996). Electric field suppression of epileptiform activity in hippocampal slices. *Journal of Neurophysiology*, 76(6):4202–4205.

Grewe, B. F., Langer, D., Kasper, H., Kampa, B. M., and Helmchen, F. (2010). High-speed in vivo calcium imaging reveals neuronal network activity with near-millisecond precision. *Nature methods*, 7(5):399.

Ho, K.-A., Bai, S., Martin, D., Alonzo, A., Dokos, S., Puras, P., and Loo, C. K. (2014). A pilot study of alternative transcranial direct current stimulation electrode montages for the treatment of major depression. *Journal of affective disorders*, 167:251–258.

Huang, Y., Liu, A. A., Lafon, B., Friedman, D., Dayan, M., Wang, X., Bikson, M., Doyle, W. K., Devinsky, O., and Parra, L. C. (2017). Measurements and models of electric fields in the in vivo human brain during transcranial electric stimulation. *Elife*, 6:e18834.

Jackson, M. P., Rahman, A., Lafon, B., Kronberg, G., Ling, D., Parra, L. C., and Bikson, M. (2016). Animal models of transcranial direct current stimulation: methods and mechanisms. *Clinical Neurophysiology*, 127(11):3425–3454.

Jamil, A., Batsikadze, G., Kuo, H.-I., Labruna, L., Hasan, A., Paulus, W., and Nitsche, M. A. (2017). Systematic evaluation of the impact of stimulation intensity on neuroplastic after-effects induced by transcranial direct current stimulation. *The Journal of physiology*, 595(4):1273–1288.

Joucla, S. and Yvert, B. (2009). The "mirror" estimate: an intuitive predictor of membrane polarization during extracellular stimulation. *Biophysical journal*, 96(9):3495–3508.

Kayyali, H. and Durand, D. (1991). Effects of applied currents on epileptiform bursts in vitro. *Experimental neurology*, 113(2):249–254.

Kuo, H.-I., Bikson, M., Datta, A., Minhas, P., Paulus, W., Kuo, M.-F., and Nitsche, M. A. (2013). Comparing cortical plasticity induced by conventional and high-definition 4× 1 ring tdcs: a neurophysiological study. *Brain Stimulation: Basic, Translational, and Clinical Research in Neuromodulation*, 6(4):644–648.

Lang, N., Siebner, H. R., Ward, N. S., Lee, L., Nitsche, M. A., Paulus, W., Rothwell, J. C., Lemon, R. N., and Frackowiak, R. S. (2005). How does transcranial dc stimulation of the primary motor cortex alter regional neuronal activity in the human brain? *European Journal of Neuroscience*, 22(2):495–504.

Lee, K. J., Queenan, B. N., Rozeboom, A. M., Bellmore, R., Lim, S. T., Vicini, S., and Pak, D. T. (2013). Mossy fiber-ca3 synapses mediate homeostatic plasticity in mature hippocampal neurons. *Neuron*, 77(1):99–114.

Loo, C. K., Alonzo, A., Martin, D., Mitchell, P. B., Galvez, V., and Sachdev, P. (2012). Transcranial direct current stimulation for depression: 3-week, randomised, sham-controlled trial. *The British Journal of Psychiatry*, 200(1):52–59.

Matsunaga, K., Nitsche, M. A., Tsuji, S., and Rothwell, J. C. (2004). Effect of transcranial dc sensorimotor cortex stimulation on somatosensory evoked potentials in humans. *Clinical Neurophysiology*, 115(2):456–460.

Mattson, M. P. and Kater, S. B. (1987). Calcium regulation of neurite elongation and growth cone motility. *Journal of Neuroscience*, 7(12):4034–4043.

Miranda, P. C., Lomarev, M., and Hallett, M. (2006). Modeling the current distribution during transcranial direct current stimulation. *Clinical neurophysiology*, 117(7):1623–1629.

Monai, H. and Hirase, H. (2017). Astrocytes as a target of transcranial direct current stimulation (tdcs) to treat depression. *Neuroscience research*.

Monte-Silva, K., Kuo, M.-F., Hessenthaler, S., Fresnoza, S., Liebetanz, D., Paulus, W., and Nitsche, M. A. (2013). Induction of late ltp-like plasticity in the human motor cortex by repeated non-invasive brain stimulation. *Brain Stimulation: Basic, Translational, and Clinical Research in Neuromodulation*, 6(3):424–432.

Ngernyam, N., Jensen, M. P., Arayawichanon, P., Auvichayapat, N., Tiamkao, S., Janjarasjitt, S., Punjaruk, W., Amatachaya, A., Aree-uea, B., and Auvichayapat, P. (2015). The effects of transcranial direct current stimulation in patients with neuropathic pain from spinal cord injury. *Clinical Neurophysiology*, 126(2):382–390.

Nitsche, M. A., Boggio, P. S., Fregni, F., and Pascual-Leone, A. (2009). Treatment of depression with transcranial direct current stimulation (tdcs): a review. *Experimental neurology*, 219(1):14–19.

Nitsche, M. A., Fricke, K., Henschke, U., Schlitterlau, A., Liebetanz, D., Lang, N., Henning, S., Tergau, F., and Paulus, W. (2003). Pharmacological modulation of cortical excitability shifts induced by transcranial direct current stimulation in humans. *J. Physiol. (Lond.)*, 553(Pt 1):293–301.

Nitsche, M. A. and Paulus, W. (2000). Excitability changes induced in the human motor cortex by weak transcranial direct current stimulation. *The Journal of physiology*, 527(3):633–639.

Nitsche, M. A. and Paulus, W. (2001). Sustained excitability elevations induced by transcranial dc motor cortex stimulation in humans. *Neurology*, 57(10):1899–1901.

Oray, S., Majewska, A., and Sur, M. (2004). Dendritic spine dynamics are regulated by monocular deprivation and extracellular matrix degradation. *Neuron*, 44(6):1021–1030.

Radman, T., Ramos, R. L., Brumberg, J. C., and Bikson, M. (2009). Role of cortical cell type and morphology in subthreshold and suprathreshold uniform electric field stimulation in vitro. *Brain Stimulation: Basic, Translational, and Clinical Research in Neuromodulation*, 2(4):215–228.

Ramakers, G., Avci, B., Van Hulten, P., Van Ooyen, A., Van Pelt, J., Pool, C., and Lequin, M. (2001). The role of calcium signaling in early axonal and dendritic morphogenesis of rat cerebral cortex neurons under non-stimulated growth conditions. *Developmental Brain Research*, 126(2):163–172.

Ranieri, F., Podda, M. V., Riccardi, E., Frisullo, G., Dileone, M., Profice, P., Pilato, F., Di Lazzaro, V., and Grassi, C. (2012). Modulation of ltp at rat hippocampal ca3-ca1 synapses by direct current stimulation. *Journal of neurophysiology*, 107(7):1868–1880.

Trachtenberg, J. T., Chen, B. E., Knott, G. W., Feng, G., Sanes, J. R., Welker, E., and Svoboda, K. (2002). Long-term in vivo imaging of experience-dependent synaptic plasticity in adult cortex. *Nature*, 420(6917):788.

Turrigiano, G. G. and Nelson, S. B. (2004). Homeostatic plasticity in the developing nervous system. *Nature Reviews Neuroscience*, 5(2):97.

Van Ooyen, A. (2011). Using theoretical models to analyse neural development. *Nature Reviews Neuroscience*, 12(6):311.

Wiethoff, S., Hamada, M., and Rothwell, J. C. (2014). Variability in response to transcranial direct current stimulation of the motor cortex. *Brain stimulation*, 7(3):468–475.